Twist of the mitotic spindle culminates at anaphase onset and depends on microtubule-associated proteins along with external forces

Monika Trupinić[1], Ivana Ponjavić[1], Barbara Kokanović[1], Ivan Barišić[2], Siniša Šegvić[2], Arian Ivec[3], Iva M. Tolić[1]

[1]Ruđer Bošković Institute, Zagreb, Croatia
[2]Laboratory for Pattern Recognition and Biometric Security Systems, Faculty of Electrical Engineering and Computing, University of Zagreb, Croatia
[3]Department of Physics, Faculty of Science, University of Zagreb, Croatia

ABSTRACT

Mechanical forces produced by motor proteins and microtubule dynamics within the mitotic spindle are crucial for the movement of chromosomes and their segregation into the emerging daughter cells. In addition to linear forces, rotational forces are present in the spindle, reflected in the left-handed twisted shapes of microtubule bundles that make the spindle chiral. However, the molecular origins of spindle chirality are unknown. Here we show that spindles are most twisted at the beginning of anaphase, and reveal multiple molecular players involved in spindle chirality. Inhibition of Eg5/kinesin-5 in a non-cancer cell line abolished spindle twist and depletion of Kif18A/kinesin-8 resulted in a right-handed twist, implying that these motors regulate twist likely by rotating the microtubules around one another within the antiparallel overlaps of bridging fibers. Depletion of the crosslinker PRC1 resulted in a right-handed twist, indicating that PRC1 may contribute to the twist by constraining free rotation of microtubules. Overexpression of PRC1 abolished twist, possibly due to increased torsional rigidity of the bundles. Depletion of augmin led to a right-handed twist, suggesting that twist depends on the geometry of microtubule nucleation. Round spindles were more twisted than elongated ones, a notion that we directly tested by compressing the spindle along its axis, which resulted in stronger left-handed twist, indicating a correlation between bending moments and twist. We conclude that spindle twist is controlled by multiple molecular mechanisms acting at different locations within the spindle as well as forces, and propose a potential physiological role of twist in promoting passive mechanical response of the spindle to forces during metaphase.

INTRODUCTION

Cell division, a process by which a parent cell divides into two daughter cells, is a fundamental process of every life. Mitosis is a stage of the cell division that is responsible for the division of the cell nucleus and thereby the genetic material (Nurse, 2000). In order to segregate the genetic material during mitosis, the cell forms a mitotic spindle, a complex micro-structure made of microtubules and numerous associated proteins (McIntosh et al., 2012; Pavin and Tolic, 2016; Prosser and Pelletier, 2017). The spindle physically separates the chromosomes to the opposite poles of the cell and assures that each daughter cell has the same number of chromosomes as the parental cell.

The spindle is a mechanical structure that can generate and balance forces within itself. Forces in the spindle are crucial for proper spindle functioning in each phase of the mitosis. For example, kinetochore fibers exert forces necessary for the positioning of the chromosomes at the center of the spindle in a metaphase plate (Maiato et al., 2017; Pavin and Tolic, 2016) and for pulling the chromosomes apart during anaphase (Asbury, 2017). On the other hand, overlap bundles balance forces at kinetochores by acting as bridges between sister kinetochore fibers in metaphase and anaphase (Kajtez et al., 2016; Polak et al., 2017; Simunic and Tolic, 2016; Tolic, 2018; Vukusic et al., 2017), and they also regulate pole separation in anaphase (Scholey et al., 2016). All the forces in the spindle arise from the active processes of motor proteins as well as microtubule polymerization and depolymerization (Howard, 2001; Tolic-Norrelykke, 2008). Because of the highly important roles of forces within the spindle, it is crucial to understand them. Direct measurement of the forces in the spindle, although possible (Nicklas, 1983), is challenging because of the small scales involved.

Forces are also responsible for the shape of a spindle. Due to the mechanical properties of microtubules, which can be thought of as thin and elastic filaments that are inherently straight and curve under forces (Kajtez et al., 2016; Rubinstein et al., 2009), the spindle obtains its characteristic shape. This means that the spindle shape reflects the forces within it, which allows for an indirect measurement of forces by inferring them from the shapes of the microtubule bundles (Kajtez et al., 2016; Tolic et al., 2019), similarly to studies of forces and shapes of individual microtubules *in vitro* (Dogterom and Yurke, 1997; Gittes et al., 1993).

Recently, it was shown that the shape of the mitotic spindle in human cells is chiral as the spindle has a left-handed twist around the pole-to-pole axis (Novak et al., 2018). Microtubule bundles twist because of the forces and torques that exist within them, as well as the elastic properties of microtubule bundles. The experimentally measured three-dimensional shapes of the microtubule bundles were used to deduce forces and torques in the spindle by comparison with a theoretical model (Novak et al., 2018).

The spindle twist is potentially generated by motor proteins that, in addition to linear forces, also exert rotational forces on microtubule bundles by switching protofilaments with a bias in a certain direction (Bormuth et al., 2012; Brunnbauer et al., 2012; Bugiel et al., 2015; Can

et al., 2014; Mitra et al., 2020; Mitra et al., 2018; Ramaiya et al., 2017; Vale and Toyoshima, 1988; Walker et al., 1990; Yajima and Cross, 2005; Yajima et al., 2008). Until now, only the role of kinesin-5 (Eg5) in the spindle twist has been explored and it was shown that inhibition of Eg5 led to the abolishment of the twist (Novak et al., 2018).

Previous studies have shown that multiple motor proteins can generate rotational forces on microtubules. The first molecular motor discovered to generate torque was the single-headed axonemal dynein, a force-generating protein that powers the movement of cilia and flagella. In *in vitro* gliding motility assays, surface-attached dynein motors rotated the microtubules around their axis in a clockwise motion, when viewed from the minus-end of the microtubules, while translocating them in a linear fashion (Vale and Toyoshima, 1988). The same type of assay was used to show that the minus-end directed motor protein kinesin-14 (Ncd) generates torques which rotate microtubules in a clockwise direction as viewed from their minus-ends (Walker et al., 1990). Similar results were obtained in an assay with kinesin-14 in which microtubules glide along each other and it was observed that the transport microtubule moved in a helical motion in a clockwise direction (Mitra et al., 2020).

By using a gliding assay, it was shown that the plus-end directed kinesin-1 can exert torsional forces which rotate microtubules counterclockwise relative to an observer looking along the microtubule long axis toward the minus end (Yajima and Cross, 2005). In experiments where kinesin-1 motor proteins were coupled with microspheres and placed on the microtubule in a single-molecule conditions, it was shown that the motor was able to generate a torque sufficient to unidirectionally rotate the microsphere, probably with a directly-guided motor head from one binding site to the next without it moving freely through space to its next binding site (Ramaiya et al., 2017).

Counterclockwise rotation direction has also been found for the plus-end-directed motor protein kinesin-5 (Eg5), which was observed as a corkscrew motion of a sliding microtubule on surface-attached motors (Yajima et al., 2008). Heterodimeric kinesin-2, a processive kinesin involved in cargo transport, displays a broad range of pitches along the path on suspended microtubules in laser trap assays, which allow for tracking of kinesin motion on microtubules between two trapped beads in solution (Brunnbauer et al., 2012). They showed that the ability of motor proteins to generate torque is dictated by the structural integrity of the coiled coil in the neck region of the protein, meaning that the motor with a stable neck has reduced propensity to generate torque.

Gliding motility assays, as well as motility assays on freely suspended microtubules, showed a counterclockwise rotation for the plus-end-directed motor protein kinesin-8 (Kip3) (Bormuth et al., 2012; Mitra et al., 2018), while another study found that kinesin-8 can switch protofilaments in both directions (Bugiel et al., 2015). Finally, cytoplasmic dynein, a molecular motor responsible for minus-end-directed cargo transport along microtubules, moves in a bidirectional helical trajectory around suspended microtubules, generating torques (Can et al., 2014).

In this paper we show how spindle twist changes through different phases of mitosis and peaks around anaphase onset in both cancer and non-cancer cell lines. We focus on a non-cancer cell line and reveal several molecular players that regulate twist. We show that inhibition of Eg5 abolished spindle twist and depletion of Kif18A/kinesin-8 resulted in a right-handed twist. These motors may regulate twist by rotating the microtubules around one another within the antiparallel overlaps of bridging fibers. In addition, Eg5 may contribute to the spindle twist by crosslinking microtubules close to the spindle pole and preventing their free rotation, which would allow the accumulation of torsional stresses with the bundles. Next, depletion of the crosslinker PRC1 resulted in a right-handed twist, indicating that PRC1 may contribute to the twist by constraining free rotation of microtubules within the bridging fibers. Overexpression of PRC1 abolished twist, which may be due to an increased number of bundled microtubules and thus increased torsional rigidity of the bundles. Depletion of augmin led to a right-handed twist, suggesting that twist may be regulated by the geometry of microtubule nucleation. We found that round spindles were more twisted than elongated ones, which we explored further by compressing the spindle along the pole-to-pole axis. This resulted in stronger left-handed twist, indicating that larger bending moments, which are characteristic of rounder spindles, are correlated with larger twist. Our work reveals that spindle twist is controlled by multiple molecular mechanisms acting at different locations within the spindle, and it can be modulated by external forces. Finally, we propose a hypothetical biological function of spindle chirality in promoting the flexibility of the spindle and its passive mechanical response to external forces.

RESULTS

Assay to measure spindle twist

To estimate the twist of the spindle, the first step was to obtain end-on view images covering the whole spindle from pole to pole. If the spindle is standing vertically with respect to the imaging plane, a z-stack of images provides an end-of view of the spindle. If the spindle is lying horizontally, a z-stack provides a side view of the spindle and needs to be transformed into the end-on view. In the end-on view, if microtubule bundles look like flower petals, this is a signature of their twisted shape (Fig. 1A).

In this work, we use 3 approaches to estimate spindle twist (Fig. 1B): 1) Visual assessment, 2) Optical flow, 3) Bundle tracing. Here we describe briefly the main concept underlying each approach together with its advantages and disadvantages, and technical details are given in the Methods section. In the visual assessment method, the spindle is observed end-on and the rotation of microtubule bundles around the pole-to-pole axis is estimated visually. If the bundles rotate clockwise when moving along the spindle axis in the direction towards the observer, the twist is left-handed, and vice versa (Fig. 1B, left). The result of our visual

assessment is whether the spindle has a strong left-handed, weak left-handed, strong right-handed, weak right-handed, or no visible twist. The advantage of this method is its trustworthiness because such coarse classification of spindles into 5 groups is reliable, whereas the main disadvantage is that the results are semi-quantitative rather than quantitative.

In the optical flow method, the movement of the signal coming from microtubule bundles is estimated automatically by comparing the signal from one z-plane to the next (Fig. 1B, middle). This method yields a value for the average twist of all bundles in a spindle. It is a preferred choice for high-throughput studies because it is automated. Disadvantages are that it provides only the average twist value instead of the twist of each bundle, and that the results are sensitive to unspecific signal in the images, individual bundles with atypical behavior, and imperfect alignment of the spindle axis with the z-axis. Visual assessment is used as a control.

In the bundle tracing method, individual bundles are manually traced by following the bundle contour in the end-on view of the spindle (Fig. 1B, right). Subsequently, each bundle is analyzed so that a plane is fitted to the points representing the bundle, and a circle that lies within this plane is fitted to the same points. From these fits, the curvature of the bundle is calculated as one over the radius, and the twist is calculated as the angle between the fitted plane and the z-axis divided by the mean distance of the points from the z-axis (Fig. 1B). The main advantage of this method is that it yields a value of twist for each individual bundle in the spindle, whereas the main disadvantage is that it requires manual tracing, which makes it inadequate for high-throughput studies.

As a label for microtubule bundles, we used SiR-tubulin to observe all microtubule bundles, or PRC1-GFP to observe the bridging fibers. To compare the results of the three methods, we analyzed twist of 10 metaphase spindles in HeLa cells stably expressing PRC1-GFP (Fig. 1C). All three methods yielded a left-handed twist, which is expressed by negative values, for all the 10 spindles. The spindles that were visually assessed as having a strong left twist had, on average, a higher left twist value also in the bundle tracing and optical flow method, than those with a weak left twist. The absolute values of twist of individual spindles obtained by bundle tracing and optical flow were similar, with optical flow yielding smaller negative values (-1.32 ± 0.29 °/μm, n = 10; all data are given as mean ± sem) than bundle tracing (-2.07 ± 0.29 °/μm, n = 10). This difference is likely due to the high sensitivity of the optical flow method for all signal, including the noisy background. Based on this cross-check between the three methods, we conclude that they provide a comparable value of spindle twist. We proceed by always using the visual assessment method and combine it with optical flow for experiments in which we test changes in the overall twist of the spindle on a large number of cells, or with bundle tracing for experiments where high spatial precision is required.

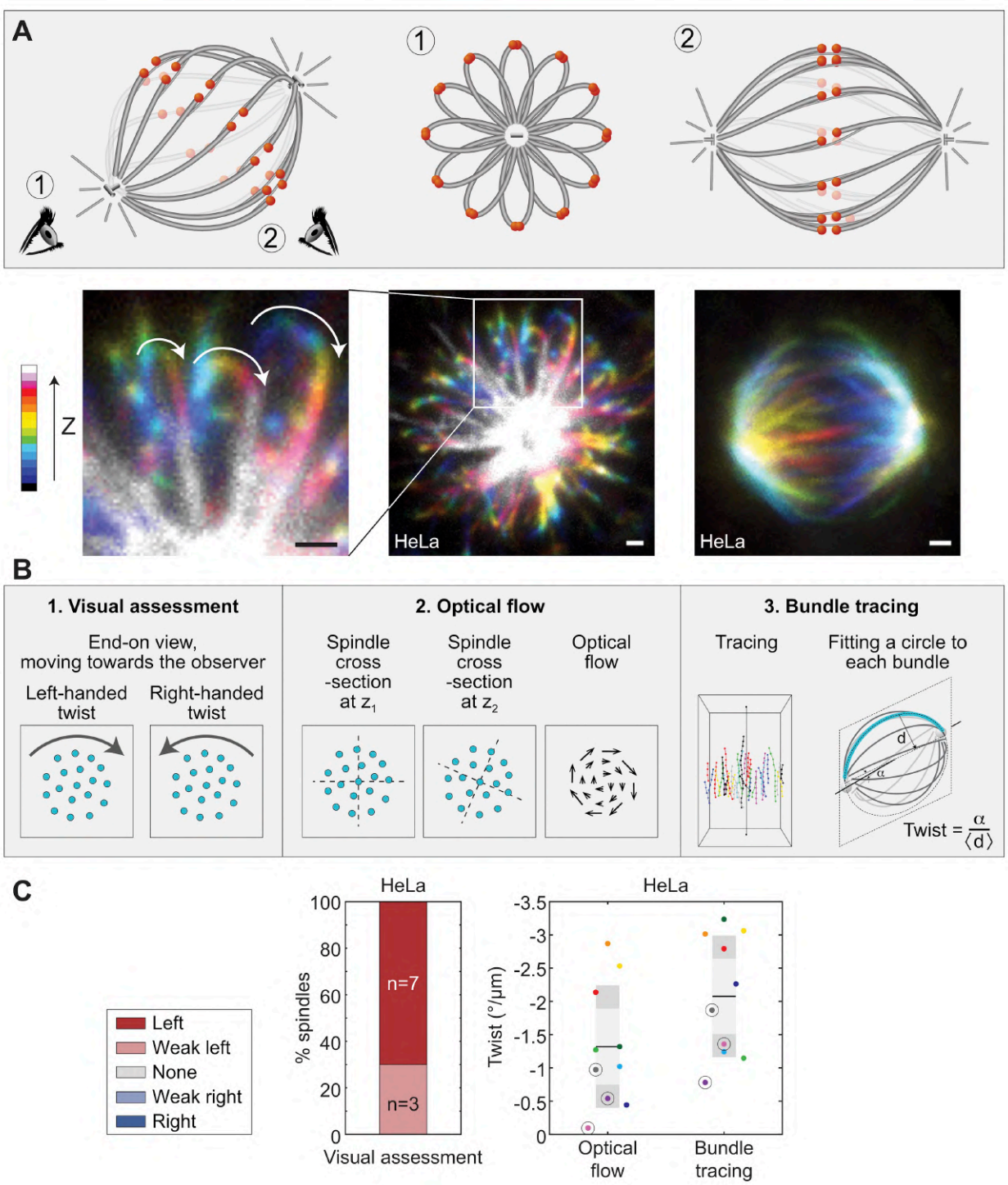

Figure 1. Visualization of the spindle twist and methods for twist calculation.

(A) On the top, simplified scheme of a spindle. A view of the spindle from an arbitrary angle is shown at the left, together with eye signs marking the view angle for the end-on view (1) and the side view (2), which are shown in the middle and on the right, respectively. Microtubule bundles are shown in grey and kinetochores in red. On the bottom, microscope images of spindles immunostained for anti-alpha tubulin

in HeLa-Kyoto BAC cell line stably expressing PRC1-GFP. Enlarged section of an image showing microtubule bundles from the end-on view, rotating in a clockwise direction through z-planes, is shown at the left. The end-on view and the side view of a spindle are shown in the middle and at the right, respectively. Images are shown in maximum z-projections and color-coded as described in the legend (using ImageJ temporal color coding Lookup Table '16 colors'). Scale bar, 1 µm.

(B) Simplified scheme of three methods used to measure spindle twist: visual assessment (1), optical flow (2) and bundle tracing (3).

(C) Comparison of the data calculated with three different methods of twist measurement. On the left, visual assessment graph represents percentages of spindles showing left, right, weak left, weak right or none twist as described in the legend. On the right, graph shows twist values calculated with optical flow and bundle tracing methods; each color represents one cell; circled and un-circled data correspond with the 'weak left' and 'left' data from the visual assessment graph, respectively. The black line shows the mean; the light and dark grey areas mark 95% confidence interval on the mean and standard deviation, respectively. Same cells were used to calculate the data for both methods. Experiments were performed on the HeLa-Kyoto BAC cells stably expressing PRC1-GFP (n=10).

Spindle twist culminates at anaphase onset in cancer and non-cancer cell lines

To examine how the spindle twist changes throughout mitosis, we measured twist in individual live HeLa cells expressing PRC1-GFP as they progress through mitosis (Fig. 2A, 2B; Fig. S1). We found that the average twist of the spindle in prometaphase is close to 0, it increases during metaphase, culminates at anaphase onset reaching a value of -1.88 ± 0.3 °/µm (n = 5), and decreases afterwards (Fig. 2B). In agreement with this result, experiments in which different spindles were imaged in different phases showed a peak of spindle twist around anaphase onset, with a value of -1.98 ± 0.26 °/µm (n = 6) (Fig. 2C; Fig. S2).

Spindle twist has so far been measured only in human cancer cell lines, HeLa and U2OS (Novak et al., 2018). To explore whether the spindle twist is specific to cancer cell lines, we measured twist in the non-cancer immortalized epithelial cell line hTERT-RPE1 (from here on referred to as RPE1) (Fig. 2A) and found that spindles in these cells also show a left-handed twist (Fig. 2D). Moreover, the temporal pattern of twist in RPE1 cells was similar to that in HeLa cells. Twist was absent in prometaphase, it was left-handed in metaphase, had a peak value at anaphase onset, decreased during anaphase, and vanished in late anaphase (Fig. 2D). The value at anaphase onset was -0.53 ± 0.15 °/µm (n = 26), which was smaller than in HeLa cells.

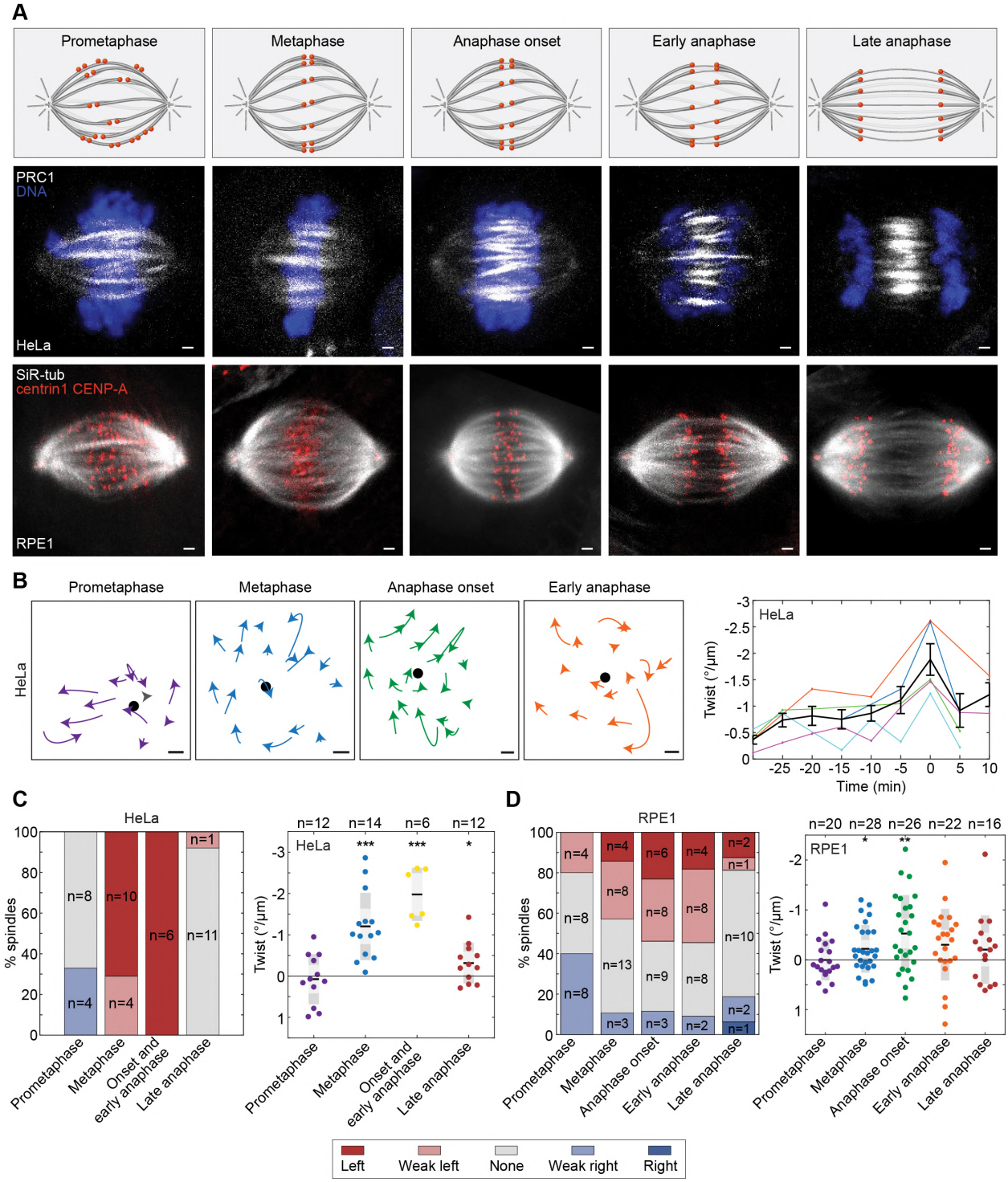

Figure 2. Spindle twist culminates at the beginning of the anaphase.

(A) On the top, simplified scheme of the mitotic spindles shown in different phases of mitosis.

In the middle, microscope images of spindles in HeLa-Kyoto BAC cells stably expressing PRC1-GFP, shown in different phases of mitosis. On the bottom, microscope images of spindles in hTERT-RPE1 cells, permanently transfected and stabilized using CENP-A-GFP and centrin1-GFP, shown in different

phases of mitosis. On the scheme, microtubule bundles are shown in grey and kinetochores in red. On microscope images, microtubule bundles are shown in grey (PRC1-GFP in HeLa and SiR-tub dye in RPE1), DNA (SiR-DNA dye) in blue and kinetochores/centrosomes in red. Images are shown in maximum z-projections. Scale bar, 1 µm.

(B) On the left, representation of microtubule bundle movements of the same spindle, viewed from the end-on view, in different phases of mitosis; each microtubule bundle is represented by a circular arc of the circle fitted on the traces and arrowheads which point at the rotation direction; black dot represents the pole-to-pole axis; each color represents one phase of the mitosis; scale bar, 1 µm. On the right, graph shows the change of twist values for five cells in time; the beginning of the anaphase (visible chromosome separation) was set at zero min; each color represents one cell and thick black line represents mean values with error bars representing SEM; data shown in the orange represents the cell whose bundles are shown on the graphs at the left. Experiments were performed on the HeLa-Kyoto BAC cells stably expressing PRC1-GFP.

(C) Highest twist values in HeLa cells are at the beginning of the anaphase. On the left, visual assessment graph represents percentages of spindles showing left, right, weak left, weak right or none twist, as described in the legend, in different phases of mitosis. On the right, graph shows twist values calculated with the optical flow method in different phases of mitosis. The black line shows the mean; the light and dark grey areas mark 95% confidence interval on the mean and standard deviation, respectively; n represents the number of the cells used; ***$p<0.001$, *$p<0.05$ (Student's t-test, mean twist value different from 0). Experiments were performed on the HeLa-Kyoto BAC cells stably expressing PRC1-GFP.

(D) Highest twist values in RPE1 cells are at the beginning of the anaphase. On the left, visual assessment graph represents percentages of spindles showing left, right, weak left, weak right or none twist, as described in the legend, in different phases of mitosis. On the right, graph shows twist values calculated with the optical flow method in different phases of mitosis. The black line shows the mean; the light and dark grey areas mark 95% confidence interval on the mean and standard deviation, respectively; n represents the number of the cells used; **$p<0.01$, *$p<0.05$ (Student's t-test, mean twist value different from 0). Experiments were performed on the hTERT-RPE1 cells, permanently transfected and stabilized using CENP-A-GFP and centrin1-GFP.

Inhibition of Eg5 abolishes spindle twist and depletion of Kif18A results in a right-handed twist

To explore the mechanisms that generate and regulate spindle twist, we consider the following molecular activities. First, motors that exert torque on the microtubule may generate the twisted shape of the bundle by twisting the microtubules within the bundle around each other, or by twisting the microtubule with respect to the spindle pole. Second, to prevent the free rotation of the microtubules, they need to be crosslinked within the bundle and at the spindle pole. Third, microtubule nucleation within the bundle may affect the bundle twist.

To test the role of these activities in the regulation of spindle twist, we performed a candidate screen on RPE1 cells in which we perturbed motor proteins and other microtubule-

associated proteins by using siRNA-mediated depletion, small-molecule inhibitors, or overexpression, and measured the resulting spindle twist. As the candidates for this mini-screen, we selected the motor proteins for which it has been shown *in vitro* that they can rotate the microtubule, the main crosslinker of antiparallel microtubules PRC1, and the augmin complex that is responsible for the nucleation of microtubules along existing microtubules. Spindle twist was measured during metaphase because depletion of some of the candidates, such as Kif18A, HAUS6 and HAUS8, interferes with anaphase entry (Stumpff et al., 2008; Uehara et al., 2009).

In agreement with our previous work on HeLa cells (Novak et al., 2018), we found that inhibition of Eg5 with S-trityl-L-cysteine (STLC), also abolished spindle twist in RPE1 cells by ~71% (-0.06 ± 0.19 °/µm, n = 11) (Fig. 3A, 3B). Depletion of another motor protein with side-stepping ability, Kif18A, led to the complete abolishment of the left-handed spindle twist (0.28 ± 0.14 °/µm, n = 17) and caused ~65% of total spindles to twist in the right-handed fashion (Fig. 3A, 3B). Overexpression of either Eg5 or Kif18A motor proteins did not yield any changes in twist compared to the spindles in untreated cells (Fig. 3A, 3B).

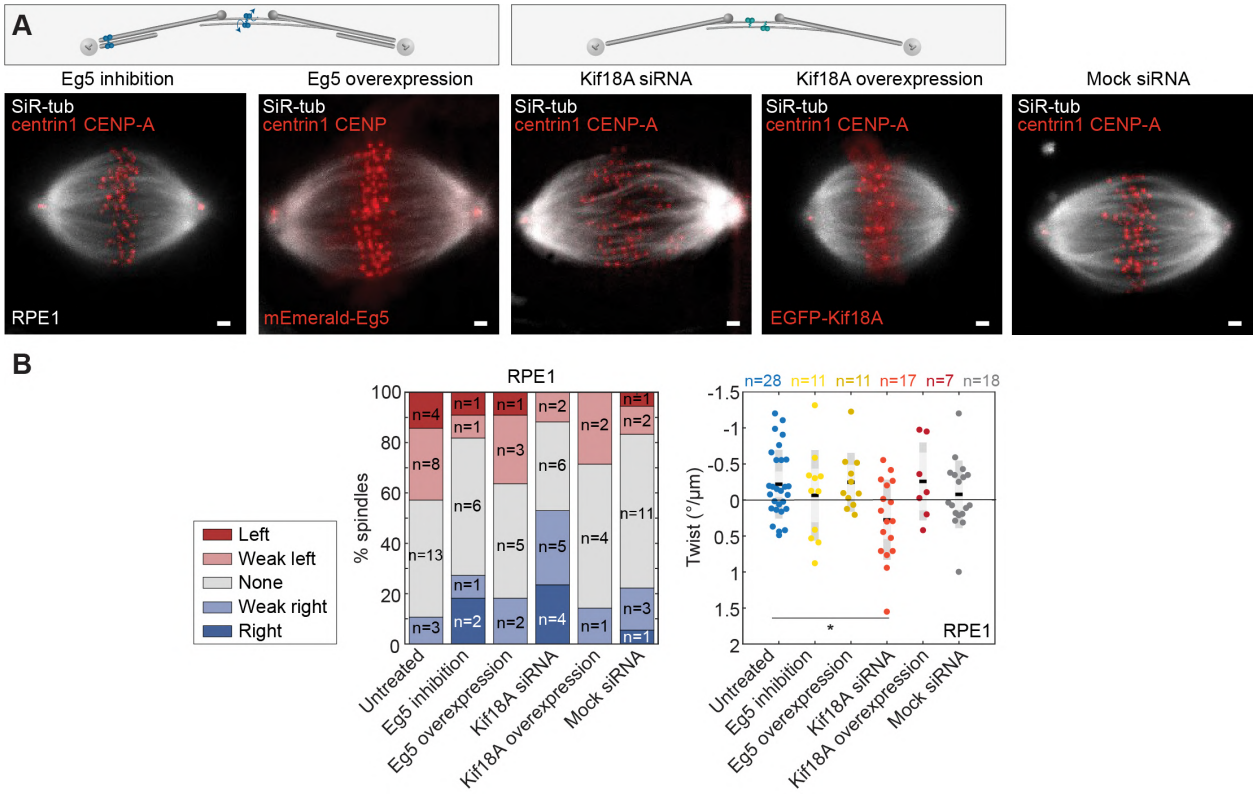

Figure 3. Inhibition/depletion of Eg5 or Kif18A abolishes left-handed spindle twist.

(A) On the top, simplified schemes of microtubule bundles extending from the opposite poles showing the position of Eg5 (left) and Kif18A (right) motor proteins. On the bottom, microscope images of the spindles in the hTERT-RPE1 cells, permanently transfected and stabilized using CENP-A-GFP and centrin1-GFP RPE1, after perturbations of Eg5 and Kif18A motor proteins. Microtubule bundles shown

in grey and kinetochores/centrosomes, Eg5 and Kif18A in red. Images are shown in maximum z-projections. Scale bar, 1 µm. Additional examples of spindles are shown in Fig. S3.
(B) Abolishment of left-handed spindle twist. On the left, visual assessment graph represents percentages of spindles showing left, right, weak left, weak right or none twist, as described in the legend, after perturbations of Eg5 and Kif18A motor proteins. On the right, graph shows twist values calculated with the optical flow method after perturbations of Eg5 and Kif18A motor proteins. The black line shows the mean; the light and dark grey areas mark 95% confidence interval on the mean and standard deviation, respectively; n represents the number of the cells used; one-way ANOVA test showed significant difference between group means ($p = 0.04$); *$p<0.05$ (Tukey's HSD post hoc test); Experiments were performed on the hTERT-RPE1 cells, permanently transfected and stabilized using CENP-A-GFP and centrin1-GFP.

Depletion of PRC1 makes the spindles twist in a right-handed manner, whereas overexpression of PRC1 abolishes twist

PRC1 protein is a key regulator of cytokinesis, but also a main crosslinking protein of antiparallel microtubules (Kajtez et al., 2016; Polak et al., 2017). As it was previously shown, removal of the PRC1 from the spindle partially disassembles bridging fibers and affects spindle shape (Jagrić et al., 2020). Without PRC1, spindles have less curved and more diamond-like shape (Jagrić et al., 2020; Kajtez et al., 2016), which led us to hypothesize that the twist might also be affected. Surprisingly, when we depleted PRC1, the spindles had right-handed twist of 0.26 ± 0.15 °/µm ($n = 14$) (Fig. 4A, 4B). In contrast, overexpression of PRC1 protein resulted in the abolishment of the spindle twist, with a complete lack of rotational movement of microtubule bundles (Fig. 4A, 4B). In this case, the optical flow method did not agree with the visual assessment method and we found that the former yielded overestimated twist values due to imperfect alignment of PRC1-overexpressing spindles and their small movements during the acquisition of the z-stack.

Depletion of augmin makes the spindles twist in a right-handed manner

Augmin complex is responsible for the recruitment of factors and proteins necessary for the microtubule nucleation from the lateral surface of the pre-existing microtubules (David et al., 2019; Uehara et al., 2009). Augmin is important for the nucleation of the bridging fibers and, consequentially, the maintenance of the spindle shape (Manenica et al., 2020). This made the augmin complex an interesting target for perturbation to determine if the spindle twist would be affected. When we depleted one of the subunits of augmin complex, HAUS6, the spindles had a right-handed twist of 0.59 ± 0.23 °/µm ($n = 14$) (Fig. 4A, 4B). A similar result was observed after the depletion of another subunit of the augmin complex, HAUS8, which resulted in an even stronger right-handed twist of 0.85 ± 0.24 °/µm ($n = 13$) (Fig. 4A, 4B).

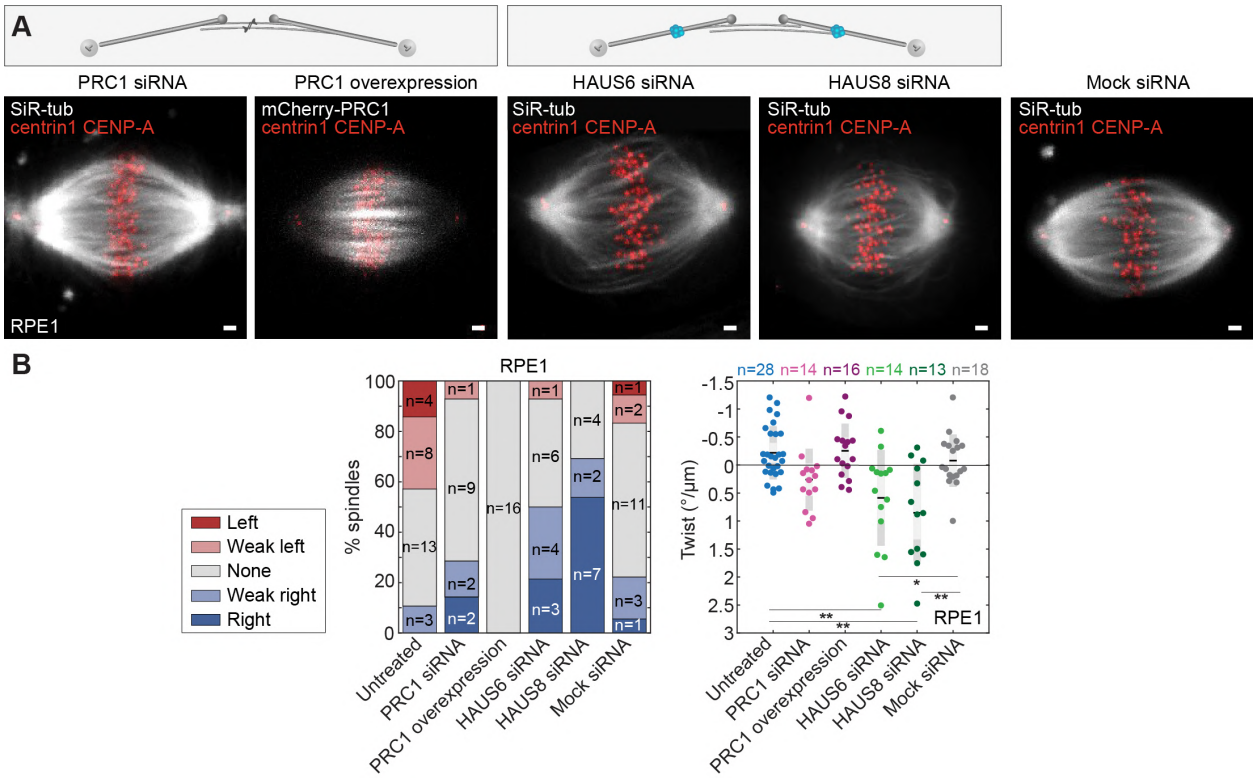

Figure 4. Depletion of PRC1 or subunits of augmin complex HAUS6 and HAUS8 abolishes left-handed spindle twist or switches it into a right-handed fashion.

(A) On the top, simplified schemes of microtubule bundles extending from the opposite poles showing the position of PRC1 protein (left) and augmin complex (right). On the bottom, microscope images of the spindles in the hTERT-RPE1 cells, permanently transfected and stabilized using CENP-A-GFP and centrin1-GFP RPE1, after perturbations of PRC1 protein and subunits of augmin complex HAUS6 and HAUS8. Microtubule bundles shown in grey (mCherry-PRC1 for PRC1-overexpressed cells and SiR-tub dye for the rest of the cells) and kinetochores/centrosomes in red. Images are shown in maximum z-projections. Scale bar, 1 µm. Additional examples of spindles are shown in Fig. S3.

(B) On the left, visual assessment graph represents percentages of spindles showing left, right, weak left, weak right or none twist, as described in the legend, after perturbations of PRC1 protein and subunits of augmin complex HAUS6 and HAUS8. On the right, graph shows twist values calculated with the optical flow method after perturbations of PRC1 protein and subunits of augmin complex HAUS6 and HAUS8. The black line shows the mean; the light and dark grey areas mark 95% confidence interval on the mean and standard deviation, respectively; n represents the number of the cells used; one-way ANOVA test showed significant difference between group means ($p = 5.52 \times 10^{7}$); *p<0.05, **p<0.01 (Tukey's HSD post hoc test); significant difference between PRC1 overexpression and HAUS6 or HAUS8 siRNA (*p<0.05 or **p<0.01, respectively) is not shown on the graph. Experiments were performed on the hTERT-RPE1 cells, permanently transfected and stabilized using CENP-A-GFP and centrin1-GFP.

Round spindles are more twisted that elongated spindles

While imaging different types of spindles (phases of mitosis, cell lines, protein perturbation etc.), we noticed that round spindles generally have stronger twist than elongated spindles. In order to quantify this observation, we took 10 HeLa cells and measured their spindle length and width and calculated the width/length ratio as a measure for the roundness of the spindle, where ratio values closer to zero describe elongated spindles and those closer to 1 more round ones (Fig. 5A). Higher width/length ratios are a signature of stronger bending moments in the spindle (Novak et al., 2018). We tested the correlation between the width/length ratios and twist values and found that rounder spindles had a stronger left-handed twist (Fig. 5A). This correlation was stronger in the results obtained by the bundle tracing method ($p < 0.05$) than by the optical flow method, due to the more precise results of the former method.

A plot of the twist as a function of the width/length ratio for various treatments indicates that different combinations of twist and bending moments exist in spindles in which different molecular mechanisms are perturbed (Fig 5B). Left-handed twist was predominantly found in spindles with higher width/length ratios, whereas right-handed twist was found in a broader interval of width/length ratios. Spindles with the lowest width/length ratios were twisted in a right-handed direction.

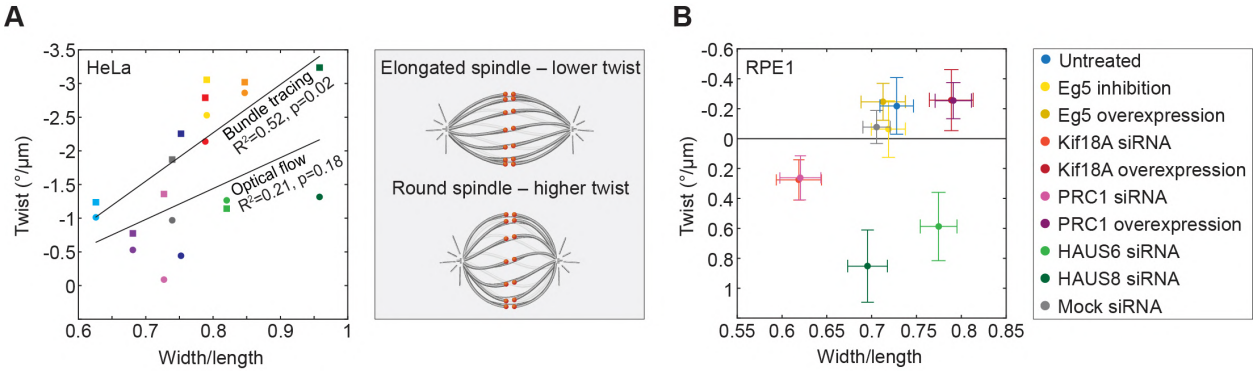

Figure 5. Round spindles have stronger twist than elongated spindles.
(A) On the left, graph shows the correlation between width/length ratio and twist; results are calculated with both the optical flow and bundle tracing method. Each color represents one cell (n=10), where dots represent the data obtained with the optical flow method and squares represent the data obtained with the bundle tracing method. Color of each data matches the color of the same data in graph in Fig. 1C. Black lines show linear fit for each method; equations y=4.59x-2.23 for optical flow and y=7.18x-3.48 for bundle tracing; goodness of fit shown in the graph. Same cells were used for both methods. Experiments were performed on the HeLa-Kyoto BAC cells stably expressing PRC1-GFP. Colors of the cells match the colors of the same cells in Fig. 1C. On the right, simplified scheme showing elongated and round spindle, with lower and higher width/length ratio, respectively. Microtubule bundles are shown in grey and kinetochores in red.

(B) Graph showing how the spindle twist and width/length ratio in RPE1 cells vary depending on the different perturbations of spindle-associated proteins. Each color represents different protein perturbation, as described in the legend, and colors match with the colors of perturbations in the Fig. 3B and 4B, from which the data was taken; dots represent mean values with error bars representing SEM. Experiments were performed on the hTERT-RPE1 cells, permanently transfected and stabilized using CENP-A-GFP and centrin1-GFP.

Compression of the spindle along the pole-to-pole axis increases the left-handed twist

As the biological role of the spindle twist is still mysterious, we hypothesized that the twisted shape may help to maintain the robustness of the spindle under force perturbations. To test this idea, we compressed vertically oriented HeLa cell spindles along the pole-to-pole axis for 1.5 minute, following the compression protocol from a previous study (Dumont and Mitchison, 2009) (Fig. 6A). Here, we used the bundle tracing method to measure spindle twist, curvature and length, which allowed us to graphically reconstruct spindles from the end-on view and side view. Traces of the microtubule bundles in the end-on view after 1 minute of compression were more rounded than before compression and the mitotic spindle shortened (Fig. 6B). The measure that we used for validation of the compression was spindle length, which decreased ~21% from 13.85 ± 0.74 μm before compression to 10.93 ± 2.31 μm after 1 minute of compression ($p = 0.25$) (Fig. 6C). Interestingly, compression resulted in a ~102% increase of the left-handed spindle twist, from -1.03 ± 0.19 °/μm before compression to -2.08 ± 0.44 °/μm after 1 minute of compression ($p = 0.03$) (Fig. 6C), and did not cause ruptures of the spindles, which supports the idea that twist helps to maintain the spindle form even when an external force is acting upon the spindle. We also measured the contour length of the microtubule bundles, which is equal to the length of the fitted circular arcs plus the distance of bundle ends from the corresponding poles. Contour length did not significantly change after compression (17.92 ± 1.18 μm before compression and 18.48 ± 2.41 μm after 1 minute of compression, which is a ~3% increase, $p = 0.183$) (Fig. 6C). Bundle curvature also did not change after compression (0.103 ± 0.009 1/μm before compression and 0.095 ± 0.009 1/μm after 1 minute of compression) (Fig. 6C).

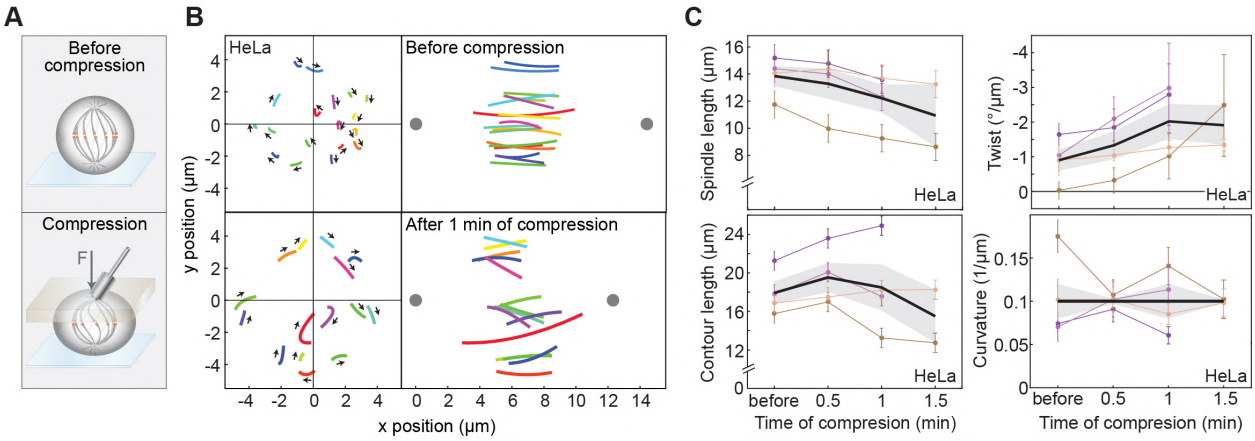

Figure 6. Spindles compressed by an external force have stronger twist.
(A) Simplified scheme of the experimental method of a spindle compression. Blue layer represents the dish; spindle is shown inside a cell; microtubule bundles are shown in grey and kinetochores in red; grey layer represents the gel; metal rod is shown on the top of the gel; arrow represents the direction of the external force used for the compression.
(B) Microtubule bundles from the spindle shown from the end-on view (left) and side view (right). Each bundle is represented by a different color; lines show circular arcs of the fitted circles and arrows represent the rotation direction of each bundle. Grey dots in the side view represent spindle poles.
(C) On the left, graphs show the change of spindle length (top) and the length of the bundle contours (bottom) before and up to 1.5 min after the compression. On the right, graphs show the change of spindle twist (top) and curvature (bottom) before and up to 1.5 min after the compression. Each color represents one cell; dots represent mean values with error bars showing SEM. Error bars in the graphs showing spindle and contour lengths represent SEM values that we estimated to be our error in determining spindle poles (1 µm). Thick black line shows total mean with grey area representing SEM. Experiments were performed on the HeLa-Kyoto BAC cells stably expressing PRC1-GFP. Individual data points are shown in Fig. S4.

DISCUSSION

Mechanisms that generate spindle twist

In this work we reveal several molecular players and forces involved in the regulation of spindle chirality, suggesting that spindle twist is controlled by different mechanisms acting at different locations within the spindle. We performed a candidate screen in which we perturbed motor proteins and other microtubule-associated proteins, and measured the resulting spindle twist. Intriguingly, the strongest effect was obtained by depletion of the HAUS6 and HAUS8 subunits of the augmin complex, which promotes nucleation of new microtubules from the wall of existing microtubules (David et al., 2019; Goshima et al., 2008; Uehara et al., 2009). This

depletion resulted in a switch in the direction of the average spindle twist from left-handed to right-handed. How could augmin regulate the twist of microtubule bundles? It is known that the axis of the newly nucleated microtubule by the augmin complex is at angle of 0-30 degrees with respect to the axis of the old microtubule (Kamasaki et al., 2013; Petry et al., 2013) (Fig. 7A, box 1, side view). Within the spindle, the new microtubule may become laterally crosslinked with the old one (Kamasaki et al., 2013), but it is unclear whether the two microtubules are perfectly parallel to each other in the bundled state. We speculate that augmin may nucleate the new microtubule at an angle with respect to the wall of the old microtubule (Fig. 7A, box 1, front view). If the new microtubules extend skewed from the old microtubules and spiral around them, this may lead to the twist of the entire microtubule bundle.

The change of the direction of twist from left-handed to right-handed upon augmin depletion and several other perturbations hints at the existence of competing mechanisms promoting twist in the opposite directions. Different protein perturbations may tip the balance one way or the other. What determines the direction of the spindle twist in normal and perturbed spindles remains an intriguing topic for future studies.

Similarly to augmin perturbation, depletion of the crosslinker of antiparallel microtubules PRC1 led to abolishment of left-handed twist and appearance of right-handed twist in a subset of spindles. We propose that in a metaphase spindle the microtubules crosslinked by PRC1 cannot rotate freely within the bundle, resulting in the accumulation of torsional stresses (Fig. 7A, box 2). Yet the torsional rigidity of the whole bundle is low enough to allow for twisting of the bundle. In contrast, in late anaphase and in experiments with PRC1 overexpression in metaphase, the bundles had completely straight shapes. We speculate that in those cases the high amount of PRC1 within the bundles results in an increased number of bundled microtubules, which in turn increases the torsional rigidity of the bundle making it harder to twist.

Torsional stresses within the bundles are most likely generated by motor proteins. We found that inactivation of Eg5 or depletion of Kif18A abolished the left-handed twist, with presence of right-handed twist in a subset of spindles after Kif18A depletion. Both of these motors are known to exert torque on the microtubules *in vitro* (Bormuth et al., 2012; Mitra et al., 2018; Yajima et al., 2008), and are found within the antiparallel overlaps of bridging microtubules in the spindle (Jagrić et al., 2020; Kajtez et al., 2016; Mann and Wadsworth, 2018). Thus, we suggest that they generate the twisted shape of the bundle by rotating the antiparallel microtubules within the bundle around each other (Fig. 7A, box 2). Eg5 may also contribute to spindle twist by acting at the spindle pole (Fig. 7A, box 3), because the most pronounced localization of Eg5 is in the pole region (Kajtez et al., 2016; Mann and Wadsworth, 2018). Here, Eg5 may crosslink parallel microtubules (Valentine et al., 2006; Walczak et al., 1998), which would prevent their free rotation within the bundle and promote the accumulation of torsional stresses. Additionally, other motors localized at the pole may contribute to spindle twist by rotating the microtubules with respect to the spindle pole (Fig. 7A, box 3).

Forces within or outside the spindle also regulate spindle twist (Fig. 7A, box 4). We found that among the spindles in HeLa cells, which show different shapes during metaphase, round spindles are more twisted than elongated ones. In agreement with this, spindles in metaphase and just after anaphase onset are more round and more twisted than in prometaphase and late anaphase, when the spindles are elongated and twist is absent. Moreover, when we squeezed the spindles along the pole-to-pole axis, they became more round and their twist increased. These findings suggest that bending moments, which are reflected in the ratio of spindle width and length (Novak et al., 2018), are correlated with twist. Thus, the motor-based mechanisms that generate larger bending moments, making the spindle more round, may result also in larger twisting moments, visible as stronger twist of the microtubule bundles.

Physiological function of spindle twist

Spindle chirality may be simply a side-effect of the action of motors that generate torque, but it is also possible that the twisted shapes of microtubule bundles contribute to spindle function. We speculate that the slightly twisted shape observed during metaphase is beneficial for the spindle because it allows changes of spindle shape as a passive mechanical response to external forces. In this picture, a twisted spindle can quickly shorten under compressive forces by passively increasing the twist in a manner similar to an elastic spring (Fig. 7B, top). This response does not require depolymerization of spindle microtubules. In contrast, for non-twisted spindles, the straight microtubule bundles in the inner part of the spindle would need to shorten as the spindle shortens. Our experiments in which we compressed the spindle along the pole-to-pole axis and observed an increase in twist as the spindle shortened, while the contour length of microtubule bundles remained largely unchanged, provides support for the model in which the twisted shape helps the spindle to respond to forces.

In contrast, during late anaphase, the spindle is not chiral as the bundles lose their twist and become straight. This straightening occurs primarily due to the accumulation of PRC1 and also other midzone proteins within these bundles. We speculate that the straight shapes of the bundles are beneficial for the spindle in this phase to make the spindle mechanically robust and keep the chromosomes well separated (Fig. 7B, bottom).

Additional putative functions of spindle twist may be to promote physical separation of adjacent bundles during prometaphase or to help start spindle elongation at the onset of anaphase, which await further explorations. Overall, we expect that the results presented here will motivate exciting new research on the molecular mechanisms and the biological roles of rotational forces in the spindle.

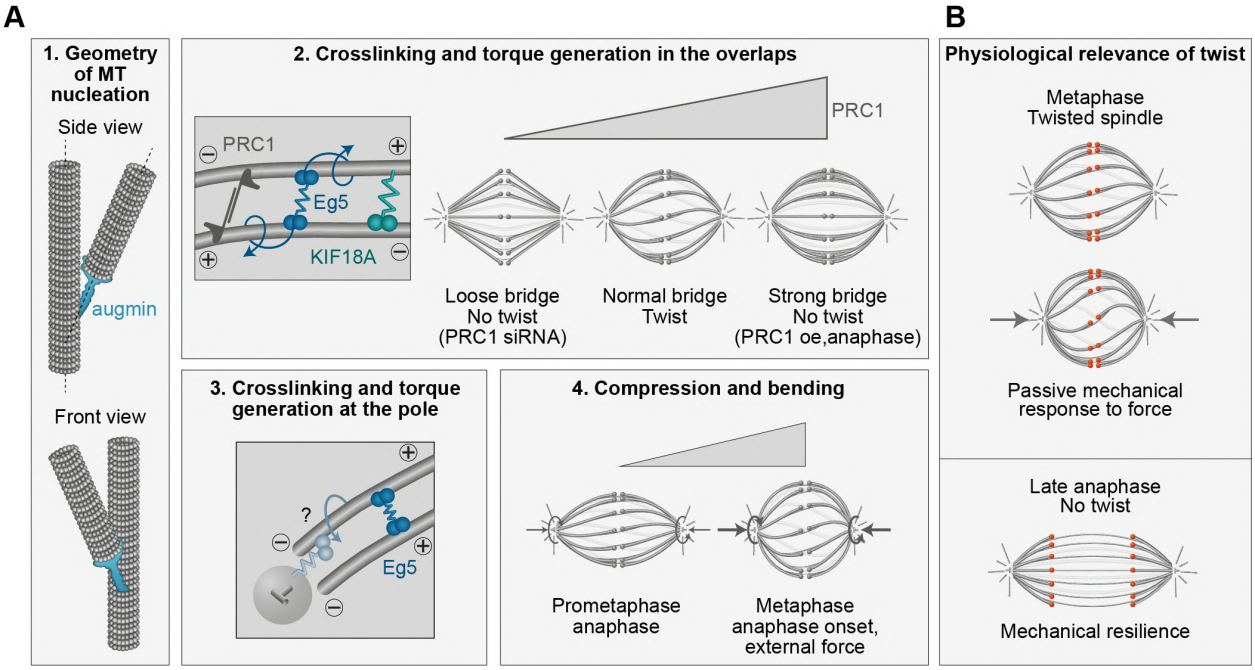

Figure 7. Model for the generation of spindle twist and its hypothetical biological role.

(A) We propose that twist is controlled by several mechanisms acting at several locations with the spindle. Augmin-mediated microtubule nucleation controls twist potentially by the skewed nucleation of a new microtubule from the old one (box 1). Within the antiparallel overlaps of bridging fibers, Eg5 and Kif18A rotate the microtubules around one another, whereas crosslinking by PRC1 constrains the free rotation of microtubules within the bundle, allowing for accumulation of torsional stresses (box 2). At the spindle pole, Eg5 crosslinks parallel microtubules, which may prevent their free rotation, and other motors may rotate the microtubules around the pole (box 3). Forces also regulate twist (box 4). Round spindles or those compressed by external forces are more twisted than elongated ones, suggesting that larger bending moments are correlated with larger twist.

(B) Potential biological role of spindle twist may be to promote passive mechanical response to external forces during metaphase. In contrast, in late anaphase twist is absent, which may promote spindle rigidity and maintenance of chromosome separation.

MATERIALS AND METHODS

Cell lines

Experiments were performed using: HeLa-Kyoto BAC cell line stably expressing PRC1-GFP courtesy of Ina Poser and Tony Hyman (Max Planck Institute of Molecular Cell Biology and Genetics, Dresden, Germany); human hTERT-RPE1 permanently transfected and stabilized using CENP-A-GFP and centrin1-GFP courtesy of Alexey Khodjakov (Wadsworth Center, New York State Department of Health, Albany, NY). Cells were grown in flasks in Dulbecco's modified Eagle's medium (DMEM; Capricorn Scientific GmbH, Germany) supplemented with 10% fetal bovine serum (FBS; Sigma-Aldrich, MO, USA), 10000 U/ml penicillin/streptomycin solution (Capricorn Scientific GmbH, Germany), and for HeLa-Kyoto BAC cells also 50 μg/mL geneticin (Life Technologies, Waltham, MA, USA). The cells were kept at 37 °C and 5% CO2 in a Galaxy 170S CO2 humidified incubator (Eppendorf, Hamburg, Germany) and regularly passaged at the confluence of 70-80%.

Sample preparation

To visualize microtubules in experiments on RPE1 cells, silicon rhodamine (SiR)-tubulin (λ_{Abs} 652 nm, λ_{Em} 674 nm) (Spirochrome AG, Stein am Rhein, Switzerland) dye was added to the dish at the final concentration of 100 nM, 2-3 hours prior to imaging. To visualize chromosomes and determine phase of the mitosis of the spindle in experiments on HeLa PRC1-GFP cells, 1 h prior to imaging silicon rhodamine (SiR)-DNA (λ_{Abs} 652 nm, λ_{Em} 674 nm) (Spirochrome AG, Stein am Rhein, Switzerland) was added to the dish at a final concentration of 100 nM. Lipofectamine RNAiMAX reagent (Invitrogen by Thermo Fisher Scientific, MA, USA) was used for RNAi treatments following manufacturer's instructions. Transfections with siRNA were always performed 48h prior to imaging at the final concentration of 100 nM. For the inhibition of Eg5, cells were treated with (+)-S-Trityl-L-cysteine (STLC, Sigma-Aldrich, MO, USA) at the final concentration of 40 μM right before the imaging so that cells are not yet collapsed into a monopol during imaging. For depletion of endogenous Kif18A, cells were transfected with Kif18A Silencer Select siRNA (4390825, Ambion, Thermo Fisher Scientific, MA, USA). In mock experiments cells were transfected with equal amount of Silencer Select Negative Control #1 siRNA (4390843, Ambion, Thermo Fisher Scientific, MA, USA). For depletion of endogenous PRC1, cells were transfected with ON-TARGETplus SMARTpool Human PRC1 (L-C19491-00-0010, Dharmacon, CO, USA). For depletions of endogenous HAUS6 and HAUS8, cells were transfected with ON-TARGETplus SMARTpool Human HAUS6 (L-018372-01-0005, Dharmacon, CO, USA) and ON-TARGETplus SMARTpool Human HAUS8 (L-031247-01-0005, Dharmacon, Co, USA), respectively. In mock experiments cells were transfected with equal amount of ON-TARGETplus Control Pool Non-Targeting pool (D-001810-10-05, Dharmacon, CO, USA). All plasmid transfections were performed using Nucleofactor Kit R with the Nucleofactor 2b Device (Lonza, Basel, Switzerland) using Y-001

program for human HMEC cells (high efficiency). To overexpress Eg5 protein, cells were transfected with 5 μg of mEmerald-Kinesin11-N-18 plasmid (Addgene number: 54137) 24h prior to imaging. For Kif18A overexpression, cells were transfected with 5 μm of EGFP-Kif18A plasmid that was a gift from Jason Stumpff (University of Vermont, Burlington, VT, USA). To overexpress PRC1 protein, cells were transfected with 5 μg of mCherry-PRC1 plasmid that was a gift from Casper C. Hoogenraad (Utrecht University, Utrecht, Netherlands). To prepare samples for microscopy, RPE1 and HeLa cells were seeded and cultured in DMEM medium with supplements at 37 °C and 5% CO2 on uncoated 35 -mm glass coverslip dishes with 0.17-mm (1.5 coverglass) glass thickness (MatTek Corporation, Ashland, MA, USA).

Immunofluorescence

HeLa-Kyoto BAC cell line stably expressing PRC1-GFP were grown on glass-bottomed dishes (14 mm, No. 1.5, MatTek Corporation) and fixed by a microtubule-preserving mixture of 3.2% PFA (paraformaldehyde) and 0.25% GA (glutaraldehyde) in microtubule-stabilizing PEM buffer (0.1 M PIPES, 0.001 M $MgCl_2$ x 6 H_2O, 0.001 M EDTA, 0.5 % Triton-X-100) for 10 min at room temperature. After fixation with PFA and GA, for quenching, cells were incubated in 1mL of freshly prepared 0.1% borohydride in PBS (phosphate-buffered saline) for 7 min and after that in 1 mL of 100 mM NH_4Cl and 100 mM glycine in PBS for 10 min at room temperature. Cells were then washed with 1 mL of PBS, 3 times for 5 min. To block unspecific binding of antibodies, cells were incubated in 500 μL blocking/permeabilization buffer (2% normal goat serum (NGS) and 0.5% Triton-X-100 in water) for 45 min at room temperature. Cells were then incubated in 500 μL of primary antibody solution (rat anti-alpha Tubulin YL1/2 (MA1-80017, Invitrogen, CA, SAD), diluted 1:500) for 24h at 4 °C. After primary antibody, cells were washed in PBS and then incubated in 500 μL of secondary antibody solution (donkey anti-rat IgG Alexa Fluor 594 (ab150156, Abcam), diluted 1:1000) for 45 min at room temperature.

Spindle compression

Spindle compression method was optimized from Mitchison and Dumont, 2009 (Dumont and Mitchison, 2009). A solution of 2 % ultra pure agarose (15510 Invitrogen by Thermo Fisher Scientific, MA, USA) in PBS was prepared, brought to boil and 2 ml was put in a 35 mm petri dish to solidify with ∼2 mm thickness. A 1 cm × 1 cm pad area was cut out, soaked in L-15 medium overnight at 4 °C for equilibration, and warmed to 37 °C just before use. Cells were plated on 14 or 20 mm glass microwell uncoated dishes before imaging. A flat metaphase cell was chosen among 80 - 100% confluent cells for pre-perturbation imaging. After imaging of the metaphase cell before compression, the pad was deposited gently, centered on the cell. Note: it is important to do this step gently and with minimal moving of the dish so the position of the cell could stay intact. Using an oil hydraulic fine manipulator (InjectMan 4, micromanipulator with dynamic movement control, 100 – 240 V/50 – 60 Hz) and a coarse manipulator attached to the confocal microscope. A metal rod (which is a part of micromanipulator where the needle for

microinjection is inserted) was centered on the cell and lowered (z-axis) until weak contact was made with the pad (rod diameter ≫ cell diameter). The rod was lowered slowly (over ∼10 s) for several µm until the cell area expanded, and its position kept constant as the cell and spindle responses were imaged. HeLa PRC1-GFP cells were imaged every 30 seconds for 3 times which gave us 4 different times the cell was imaged at: before compression , 0.5 min after compression, 1 min after compression and 1.5 minute after compression. Cell health was monitored through the presence of the intact cell membrane and the ability of the cell to enter anaphase after perturbation.

Confocal microscopy

Live RPE1 and HeLa cells were imaged using Bruker Opterra Multipoint Scanning Confocal Microscope (Buca et al., 2017) (Bruker Nano Surfaces, Middleton, WI, USA). The system was mounted on a Nikon Ti-E inverted microscope equipped with a Nikon CFI Plan Apo VC ×100/1.4 numerical aperture oil objective (Nikon, Tokyo, Japan). During imaging, cells were maintained at 37 °C in Okolab Cage Incubator (Okolab, Pozzuoli, NA, Italy). A 22 µm slit aperture was used for RPE1 and 60 µm pinhole for HeLa cells. The xy-pixel size was 83 nm. For excitation of GFP and mCherry fluorescence, a 488 and a 561 nm diode laser line was used, respectively. For SiR-dyes, a 640 nm diode laser line was used. The excitation light was separated from the emitted fluorescence by using Opterra Dichroic and Barrier Filter Set 405/488/561/640. Images were captured with an Evolve 512 Delta EMCCD Camera (Photometrics, Tucson, AZ, USA) with no binning performed. To cover the whole metaphase spindle, z-stacks were acquired at 30–60 focal planes separated by 0.5 µm with unidirectional xyz scan mode. The system was controlled with the Prairie View Imaging Software (Bruker Nano Surfaces, Middleton, WI, USA).

Image and data analysis

Microscopy images of horizontal spindles were analyzed in Fiji Software (ImageJ, National Institutes of Health, Bethesda, MD, USA) (Schindelin et al., 2012). Only images with both spindle poles roughly in the same plane were used in analysis. Horizontal spindles were transformed into vertical orientation using a code written in R programming language in RStudio. (Method described in Novak et al. (Novak et al., 2018)). In transformed stack microtubule bundles and poles appear as blobs.

Optical flow. For the optical flow method, parts of the images containing the blobs were selected for analysis using Rectangle tool in ImageJ. In all transformed stacks only images between spindle poles were used for analysis. Transformed spindle images contained a lot of noise that was removed by using the Mexican hat filter and a threshold. The Mexican hat filter, also called the LoG (Laplacian of Gaussian) filter, was used for detection of blobs (Jin and Feng, 2014; Lowe, 2004). After applying the Mexican hat filter, a threshold was applied to the image. It removes all the pixels with intensity lower than the given threshold. Microtubule bundles of

transformed spindles were detected and traced automatically using optical flow for calculating the movement of pixels between two consecutive images. Farnebäck's two-frame motion estimation algorithm (dense optical flow algorithm) was used (Farnebäck, 2003). Only spindle poles were tracked manually using Multipoint tool in ImageJ. Helicities of mitotic spindles were calculated using algorithm called All pixels helicity algorithm. It calculates the total helicity as the average helicity of all pixels in the spindle. The code for tracing of bundles and helicity calculating was written in Python programming languange using PyCharm IDE. The external libraries used in image preprocessing, calculating helicity and visualisation are NumPy, scikit-image, Matplotib, PIL, OpenCV and SciPy. The code and instructions are available at https://gitlab.com/IBarisic/detecting-microtubules-helicity-in-microscopic-3d-mages/tree/master.

Bundle tracing. Bundles in images of spindles oriented vertically were traced manually using Multipoint tool in Fiji as described in Novak et al. (Novak et al., 2018). We convert the imaging plane (z-plane) to its corresponding z-coordinate by multiplying with the distance between successive planes set during image acquisition (0.5 μm) and by a factor of 0.81 to correct for the refractive index mismatch (Novak et al., 2018). Next, to describe the shape of a microtubule bundle, we fit a plane to the points representing the bundle. Subsequently, we fit a circle that lies in this plane to the same points. From these fits we calculate the curvature and twist of the bundle as follows: (i) The curvature is calculated as one over the radius, and (ii) the twist is calculated as the angle between the plane and the z-axis divided by the mean distance of these points from the z-axis. Bundle length was calculated as the length of the projection of the bundle trace onto the pole-to-pole axis.

Statistical analysis

Fiji was used to scale images and adjust brightness and contrast. Figures were assembled in Adobe Illustrator CS5 and CC (Adobe Systems, Mountain View, CA, USA). Graphs were plotted in MATLAB (MathWorks, Natick, MA, USA). For generation of univariate scatter plots, the open "UnivarScatter" Matlab extension was used (https://github.com/manulera/UnivarScatter). Data are given as mean ± s.e.m., unless otherwise stated. Significance of data was estimated by Student's t-test (two-tailed and two sample unequal-variance). $p < 0.05$ was considered statistically significant. Values of all significant differences are given with degree of significance indicated (*$0.01 < p < 0.05$, **$0.001 < p < 0.01$, ***$p < 0.001$). Statistically significant differences between groups of data were determined by one-way ANOVA and Tukey's HSD post hoc test, $p < 0.05$ was considered statistically significant. The number of analyzed cells and microtubule bundles is given in the respective figure panel.

REFERENCES

Asbury, C.L. 2017. Anaphase A: Disassembling Microtubules Move Chromosomes toward Spindle Poles. *Biology (Basel)*. 6.

Bormuth, V., B. Nitzsche, F. Ruhnow, A. Mitra, M. Storch, B. Rammner, J. Howard, and S. Diez. 2012. The highly processive kinesin-8, Kip3, switches microtubule protofilaments with a bias toward the left. *Biophys J*. 103:L4-6.

Brunnbauer, M., R. Dombi, T.H. Ho, M. Schliwa, M. Rief, and Z. Okten. 2012. Torque generation of kinesin motors is governed by the stability of the neck domain. *Mol Cell*. 46:147-158.

Buca, R., K. Vukusic, and I.M. Tolic. 2017. Dissection and characterization of microtubule bundles in the mitotic spindle using femtosecond laser ablation. *Method Cell Biol*. 139:81-101.

Bugiel, M., E. Bohl, and E. Schaffer. 2015. The Kinesin-8 Kip3 switches protofilaments in a sideward random walk asymmetrically biased by force. *Biophys J*. 108:2019-2027.

Can, S., M.A. Dewitt, and A. Yildiz. 2014. Bidirectional helical motility of cytoplasmic dynein around microtubules. *Elife*. 3:e03205.

David, A.F., P. Roudot, W.R. Legant, E. Betzig, G. Danuser, and D.W. Gerlich. 2019. Augmin accumulation on long-lived microtubules drives amplification and kinetochore-directed growth. *J Cell Biol*. 218:2150-2168.

Dogterom, M., and B. Yurke. 1997. Measurement of the force-velocity relation for growing microtubules. *Science*. 278:856-860.

Dumont, S., and T.J. Mitchison. 2009. Force and length in the mitotic spindle. *Curr Biol*. 19:R749-761.

Farnebäck, G. 2003. Two-Frame Motion Estimation Based on Polynomial Expansion. Springer Berlin Heidelberg, Berlin, Heidelberg. 363-370.

Gittes, F., B. Mickey, J. Nettleton, and J. Howard. 1993. Flexural rigidity of microtubules and actin filaments measured from thermal fluctuations in shape. *J Cell Biol*. 120:923-934.

Goshima, G., M. Mayer, N. Zhang, N. Stuurman, and R.D. Vale. 2008. Augmin: a protein complex required for centrosome-independent microtubule generation within the spindle. *J Cell Biol*. 181:421-429.

Howard, J. 2001. Mechanics of motor proteins and the cytoskeleton. Sinauer Associates, Sunderland, Mass. xvi, 367 p. pp.

Jagrić, M., P. Risteski, J. Martinčić, A. Milas, and I.M. Tolic. 2020. Optogenetic control of PRC1 reveals that bridging fibers promote chromosome alignment by overlap length-dependent forces. *doi: https://doi.org/10.1101/865394*.

Jin, F., and D.Z. Feng. 2014. Image Registration Algorithm Using Mexican Hat Function-Based Operator and Grouped Feature Matching Strategy. *Plos One*. 9.

Kajtez, J., A. Solomatina, M. Novak, B. Polak, K. Vukusic, J. Rudiger, G. Cojoc, A. Milas, I. Sumanovac Sestak, P. Risteski, F. Tavano, A.H. Klemm, E. Roscioli, J. Welburn, D. Cimini, M. Gluncic, N. Pavin, and I.M. Tolic. 2016. Overlap microtubules link sister k-fibres and balance the forces on bi-oriented kinetochores. *Nat Commun*. 7:10298.

Kamasaki, T., E. O'Toole, S. Kita, M. Osumi, J. Usukura, J.R. McIntosh, and G. Goshima. 2013. Augmin-dependent microtubule nucleation at microtubule walls in the spindle. *J Cell Biol*. 202:25-33.

Lowe, D.G. 2004. Distinctive image features from scale-invariant keypoints. *Int J Comput Vision*. 60:91-110.

Maiato, H., A.M. Gomes, F. Sousa, and M. Barisic. 2017. Mechanisms of Chromosome Congression during Mitosis. *Biology (Basel)*. 6.

Manenica, M., V. Štimac, I. Koprivec, J. Simunic, and I.M. Tolic. 2020. Augmin regulates kinetochore tension and spatial arrangement of spindle microtubules by nucleating bridging fibers. *doi: https://doi.org/10.1101/2020.09.10.291740*.

Mann, B.J., and P. Wadsworth. 2018. Distribution of Eg5 and TPX2 in mitosis: Insight from CRISPR tagged cells. *Cytoskeleton (Hoboken)*. 75:508-521.

McIntosh, J.R., M.I. Molodtsov, and F.I. Ataullakhanov. 2012. Biophysics of mitosis. *Q Rev Biophys*. 45:147-207.

Mitra, A., L. Meissner, R. Gandhimathi, R. Renger, F. Ruhnow, and S. Diez. 2020. Kinesin-14 motors drive a right-handed helical motion of antiparallel microtubules around each other. *Nat Commun*. 11:2565.

Mitra, A., F. Ruhnow, S. Girardo, and S. Diez. 2018. Directionally biased sidestepping of Kip3/kinesin-8 is regulated by ATP waiting time and motor-microtubule interaction strength. *Proc Natl Acad Sci U S A*. 115:E7950-E7959.

Nicklas, R.B. 1983. Measurements of the force produced by the mitotic spindle in anaphase. *J Cell Biol*. 97:542-548.

Novak, M., B. Polak, J. Simunic, Z. Boban, B. Kuzmic, A.W. Thomae, I.M. Tolic, and N. Pavin. 2018. The mitotic spindle is chiral due to torques within microtubule bundles. *Nat Commun*. 9:3571.

Nurse, P. 2000. A long twentieth century of the cell cycle and beyond. *Cell*. 100:71-78.

Pavin, N., and I.M. Tolic. 2016. Self-Organization and Forces in the Mitotic Spindle. *Annu Rev Biophys*. 45:279-298.

Petry, S., A.C. Groen, K. Ishihara, T.J. Mitchison, and R.D. Vale. 2013. Branching microtubule nucleation in Xenopus egg extracts mediated by augmin and TPX2. *Cell*. 152:768-777.

Polak, B., P. Risteski, S. Lesjak, and I.M. Tolic. 2017. PRC1-labeled microtubule bundles and kinetochore pairs show one-to-one association in metaphase. *EMBO Rep*. 18:217-230.

Prosser, S.L., and L. Pelletier. 2017. Mitotic spindle assembly in animal cells: a fine balancing act. *Nat Rev Mol Cell Biol*. 18:187-201.

Ramaiya, A., B. Roy, M. Bugiel, and E. Schaffer. 2017. Kinesin rotates unidirectionally and generates torque while walking on microtubules. *Proc Natl Acad Sci U S A*. 114:10894-10899.

Rubinstein, B., K. Larripa, P. Sommi, and A. Mogilner. 2009. The elasticity of motor-microtubule bundles and shape of the mitotic spindle. *Phys Biol*. 6:016005.

Schindelin, J., I. Arganda-Carreras, E. Frise, V. Kaynig, M. Longair, T. Pietzsch, S. Preibisch, C. Rueden, S. Saalfeld, B. Schmid, J.Y. Tinevez, D.J. White, V. Hartenstein, K. Eliceiri, P. Tomancak, and A. Cardona. 2012. Fiji: an open-source platform for biological-image analysis. *Nat Methods*. 9:676-682.

Scholey, J.M., G. Civelekoglu-Scholey, and I. Brust-Mascher. 2016. Anaphase B. *Biology (Basel)*. 5.

Simunic, J., and I.M. Tolic. 2016. Mitotic Spindle Assembly: Building the Bridge between Sister K-Fibers. *Trends Biochem Sci*. 41:824-833.

Stumpff, J., G. von Dassow, M. Wagenbach, C. Asbury, and L. Wordeman. 2008. The kinesin-8 motor Kif18A suppresses kinetochore movements to control mitotic chromosome alignment. *Dev Cell*. 14:252-262.

Tolic-Norrelykke, I.M. 2008. Push-me-pull-you: how microtubules organize the cell interior. *Eur Biophys J*. 37:1271-1278.

Tolic, I.M. 2018. Mitotic spindle: kinetochore fibers hold on tight to interpolar bundles. *Eur Biophys J*. 47:191-203.

Tolic, I.M., M. Novak, and N. Pavin. 2019. Helical Twist and Rotational Forces in the Mitotic Spindle. *Biomolecules*. 9.

Uehara, R., R.S. Nozawa, A. Tomioka, S. Petry, R.D. Vale, C. Obuse, and G. Goshima. 2009. The augmin complex plays a critical role in spindle microtubule generation for mitotic progression and cytokinesis in human cells. *Proc Natl Acad Sci U S A*. 106:6998-7003.

Vale, R.D., and Y.Y. Toyoshima. 1988. Rotation and translocation of microtubules in vitro induced by dyneins from Tetrahymena cilia. *Cell*. 52:459-469.

Valentine, M.T., P.M. Fordyce, and S.M. Block. 2006. Eg5 steps it up! *Cell Div*. 1:31.

Vukusic, K., R. Buda, A. Bosilj, A. Milas, N. Pavin, and I.M. Tolic. 2017. Microtubule Sliding within the Bridging Fiber Pushes Kinetochore Fibers Apart to Segregate Chromosomes. *Dev Cell*. 43:11-23 e16.

Walczak, C.E., I. Vernos, T.J. Mitchison, E. Karsenti, and R. Heald. 1998. A model for the proposed roles of different microtubule-based motor proteins in establishing spindle bipolarity. *Curr Biol*. 8:903-913.

Walker, R.A., E.D. Salmon, and S.A. Endow. 1990. The Drosophila claret segregation protein is a minus-end directed motor molecule. *Nature*. 347:780-782.

Yajima, J., and R.A. Cross. 2005. A torque component in the kinesin-1 power stroke. *Nat Chem Biol*. 1:338-341.

Yajima, J., K. Mizutani, and T. Nishizaka. 2008. A torque component present in mitotic kinesin Eg5 revealed by three-dimensional tracking. *Nat Struct Mol Biol*. 15:1119-1121.

ACKNOWLEDGEMENTS

We thank Ina Poser, Tony Hyman and Alexey Khodjakov for cell lines; Jason Stumpff and Casper C. Hoogenraad for plasmids; Juraj Simunić, Jurica Matković, Lucija Bujanić and Iva Buljan for their contribution in experimental work; Martina Manenica for the help with the MATLAB codes, and Ivana Šarić for the drawings. We thank all members of Tolić and Pavin groups for helpful discussions. This work was funded by the European Research Council (ERC Consolidator Grant, GA Number 647077), the Croatian Science Foundation (HRZZ project IP-2019-04-5967), and the QuantiXLie Center of Excellence, a project co-financed by the Croatian Government and European Union through the European Regional Development Fund—the Competitiveness and Cohesion Operational Programme (Grant KK.01.1.1.01.0004). We also acknowledge new support by the ERC (Synergy Grant, GA Number 855158). The work of doctoral students M.T. and A.I. have been supported in part by the “Young researchers' career development project – training of doctoral students” of the Croatian Science Foundation.

AUTHOR CONTRIBUTIONS

M.T. performed experiments on RPE1 cells, B.K. performed experiments on HeLa cells, except compression experiments, which were done by I.P. M.T., B.K. and I.P. analyzed the experimental data. I.B. and S.Š. developed the optical flow method for twist measurement. A.I. measured the twist from bundle traces. M.T. and I.M.T. wrote the manuscript, with input from I.P., B.K., and other authors. M.T. assembled the figures. I.M.T. conceived the project and supervised the experiments.

SUPPLEMENTARY INFORMATION

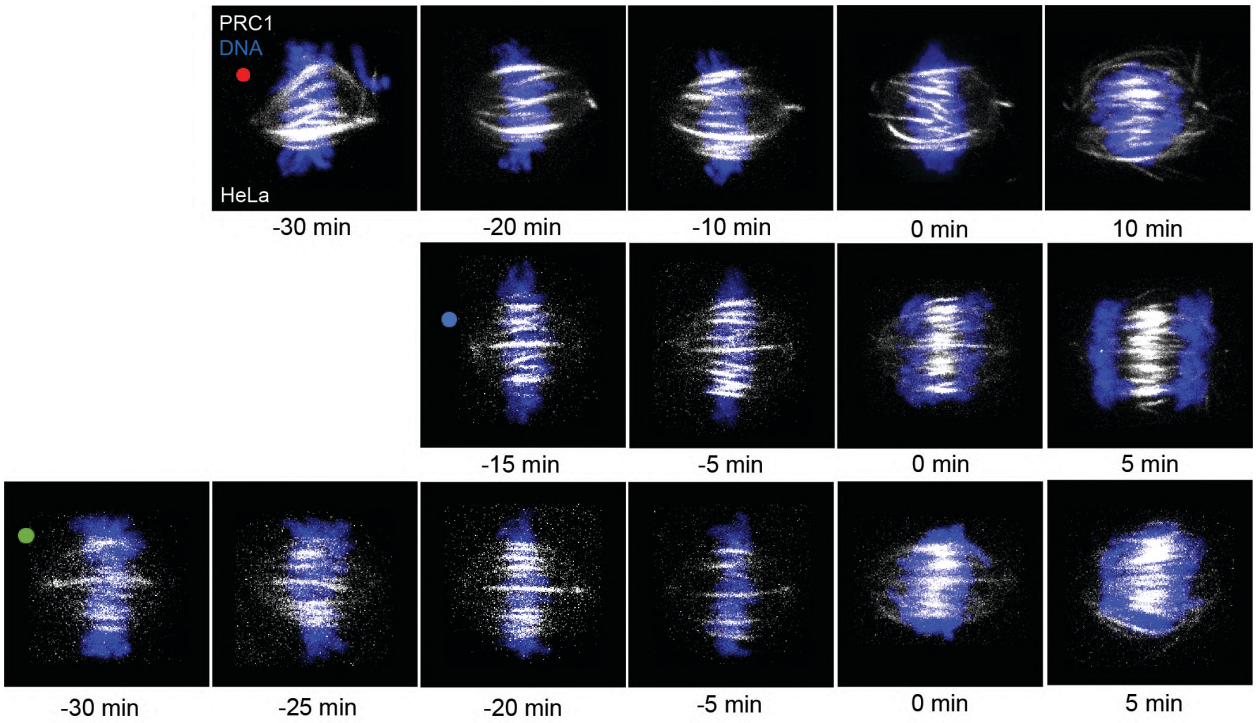

Figure S1. Progression of mitosis in HeLa spindles that were used for twist measurements. Each colored dot represents one spindle's progression in time, and each color matches the color of the spindle's data in the graph in Fig. 2B. Microtubule bundles are shown in grey (PRC1-GFP) and DNA in blue (SiR-DNA dye). Images are shown in maximum z-projections. Experiments were performed on the HeLa-Kyoto BAC cells stably expressing PRC1-GFP.

A Prometapase

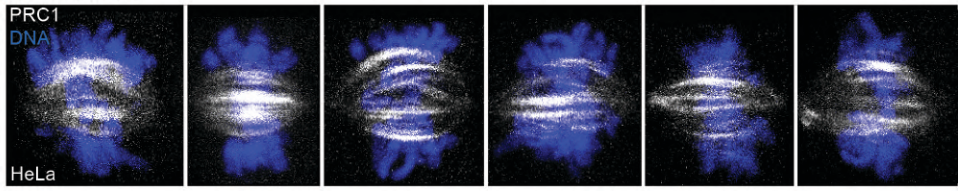

1	none	weak right	none	weak right	none	none
2	0.79 °/µm	0.13 °/µm	0.16 °/µm	-0.52 °/µm	-0.95 °/µm	-0.041 °/µm

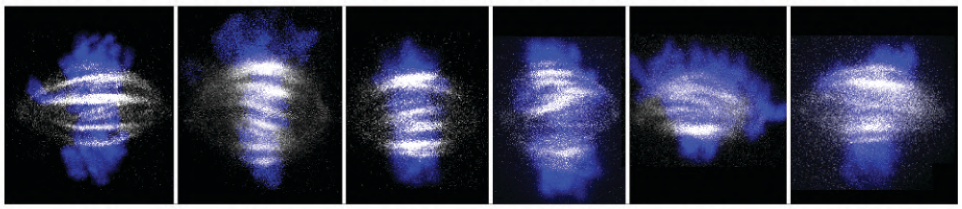

1	none	none	none	weak left	none	weak right
2	0.074 °/µm	-0.37 °/µm	0.26 °/µm	-0.52 °/µm	0.92 °/µm	0.99 °/µm

B Metapase

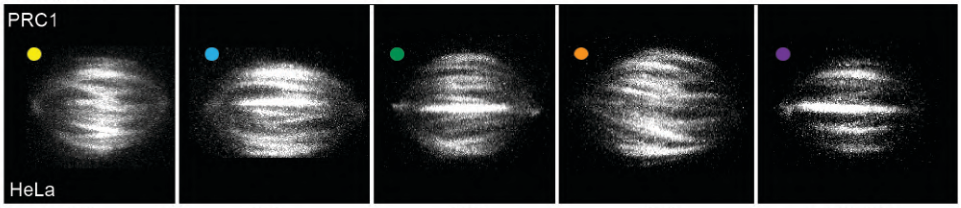

1	left	left	left	left	weak left
2	-2.5 °/µm	-1.0 °/µm	-1.3 °/µm	-2.9 °/µm	-0.53 °/µm
3	-3.1 °/µm	-1.2 °/µm	-1.1 °/µm	-3.0 °/µm	-0.78 °/µm

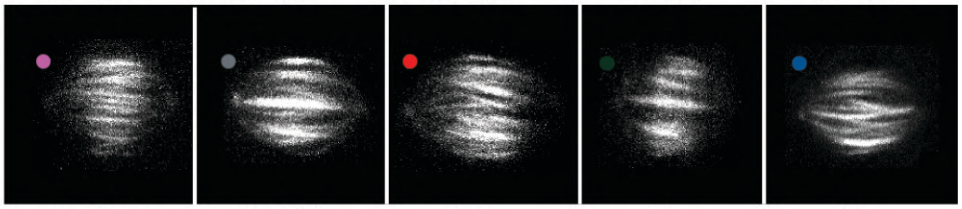

1	weak left	weak left	left	left	left
2	-0.088 °/µm	-0.97 °/µm	-2.1 °/µm	-1.3 °/µm	-0.44 °/µm
3	-1.4 °/µm	-1.9 °/µm	-2.8 °/µm	-3.2 °/µm	-2.3 °/µm

C Anaphase

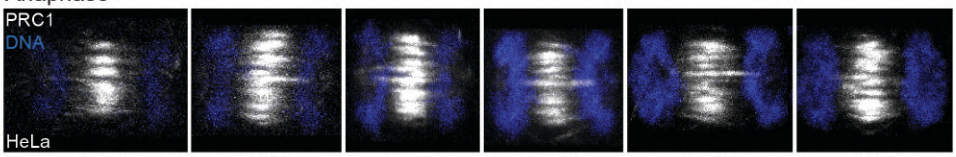

1	none	none	none	none	none	none
2	-0.46 °/µm	0.29 °/µm	-0.20 °/µm	0.030 °/µm	0.20 °/µm	0.21 °/µm

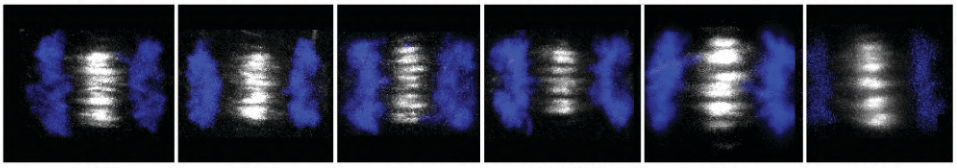

1	none	none	none	weak left	none	none
2	-0.28 °/µm	-1.4 °/µm	-0.50 °/µm	-0.78 °/µm	-0.67 °/µm	-0.19 °/µm

1 = visual assessment 2 = optical flow 3 = bundle tracing

Figure S2. HeLa spindles in different phases of mitosis have different values of twist.

(A) Different HeLa spindles with their twist values in prometaphase. Twist was determined with the visual assessment method and the optical flow, marked 1 and 2, respectively. Data was used in the graphs in Fig. 2C. Microtubule bundles are shown in grey (PRC1-GFP) and DNA in blue (SiR-DNA dye). Images are shown in maximum z-projections. Experiments were performed on the HeLa-Kyoto BAC cells stably expressing PRC1-GFP.

(B) Different HeLa spindles with their twist values in metaphase. Twist was determined with the visual assessment, optical flow and bundle tracing methods, marked 1, 2 and 3, respectively. Data was used in the graphs in Fig. 1C, 2C and 5A. Each colored dot represents one cell and matches with the color of its data shown in graphs in Fig. 1C and 5A. Microtubule bundles are shown in grey (PRC1-GFP). Images are shown in maximum z-projections. Experiments were performed on the HeLa-Kyoto BAC cells stably expressing PRC1-GFP.

(C) Different HeLa spindles with their twist values in late anaphase. Twist was determined with the visual assessment method and the optical flow, marked 1 and 2, respectively. Data was used in the graphs in Fig. 2C. Microtubule bundles are shown in grey (PRC1-GFP) and DNA in blue (SiR-DNA dye). Images are shown in maximum z-projections. Experiments were performed on the HeLa-Kyoto BAC cells stably expressing PRC1-GFP.

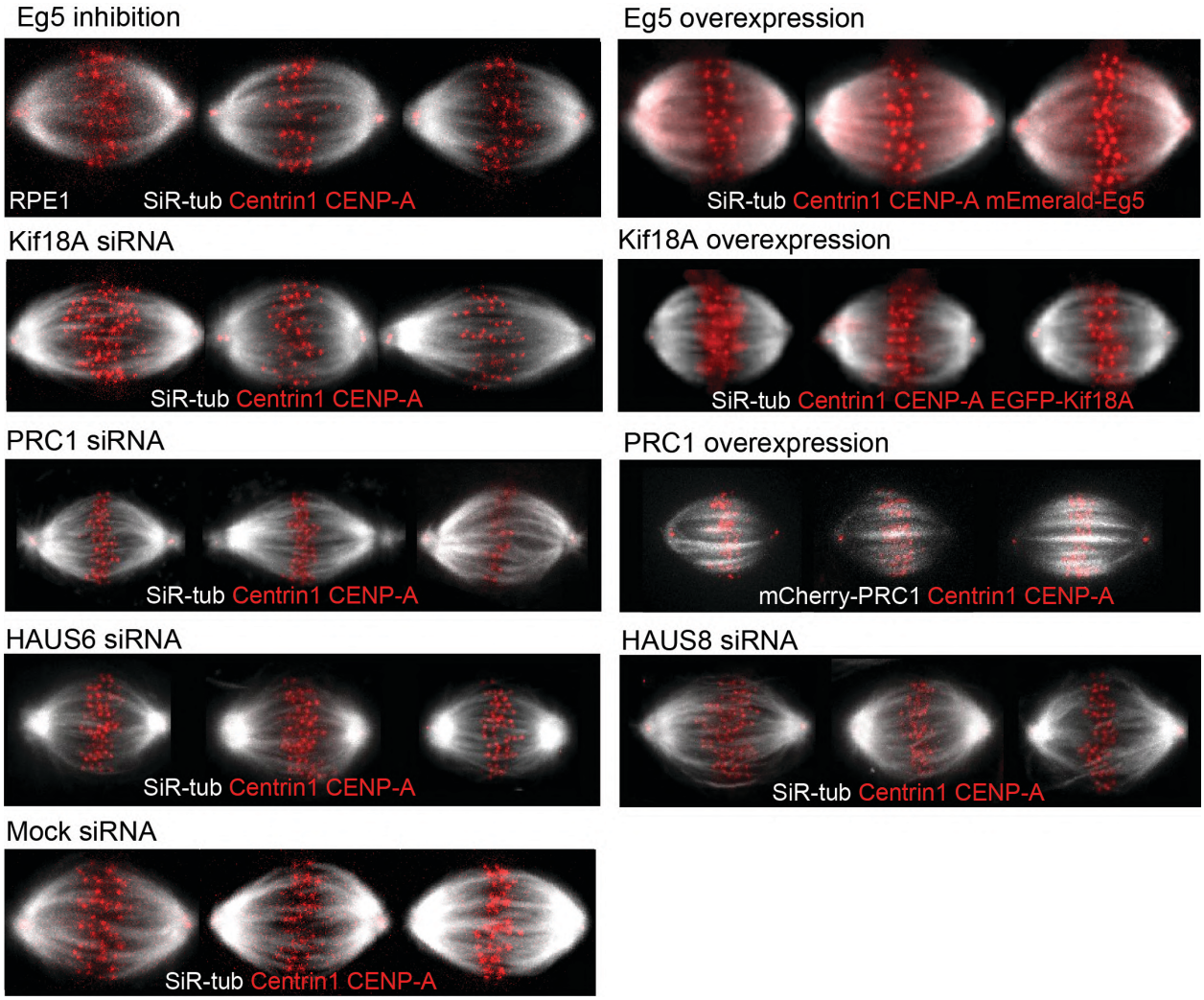

Figure S3. RPE1 spindles after perturbation of spindle-associated proteins.
Examples of three RPE1 spindles for every perturbation of spindle-associated proteins: Eg5 inhibition, Eg5 overexpression, Kif18A depletion, Kif18A overexpression, PRC1 depletion, PRC1 overexpression, HAUS6 and HAUS8 depletion ad mock control. Data was used in the graphs in Fig. 3B and 4B. Microtubule bundles are shown in grey (SiR-tub and, for PRC1 overexpression, mCherry-PRC1) and kinetochores/centrosomes, Eg5 and KiF18A in red. Images are shown in maximum z-projections. Experiments were performed on the hTERT-RPE1 cells, permanently transfected and stabilized using CENP-A-GFP and centrin1-GFP.

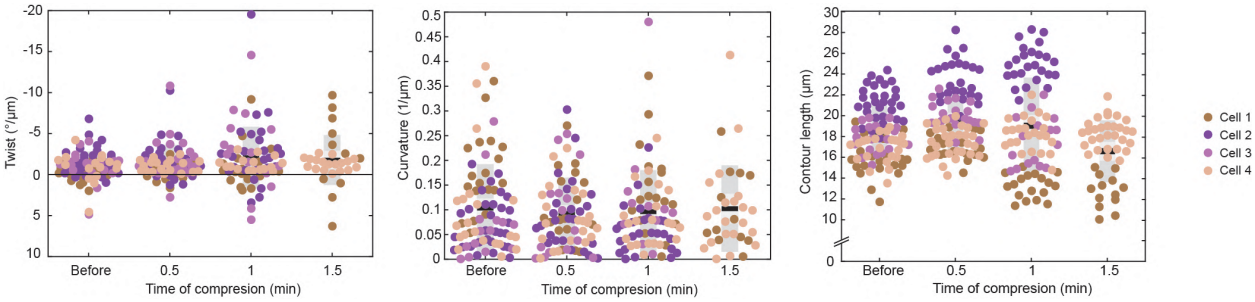

Figure S4. Twist, curvature, and contour length of microtubule bundles in spindles compressed by an external force.

On the left, graph show the change of the twist before and up to 1.5 min after the compression. In the middle, graph shows the change of the curvature before and up to 1.5 min after the compression. On the right, graph shows the change of length of the bundle contours before and up to 1.5 min after the compression. Each color represents one cell, as described in the legend; dots represent bundles; the black line shows the mean; the light and dark grey areas mark 95% confidence interval on the mean and standard deviation, respectively. Experiments were performed on the HeLa-Kyoto BAC cells stably expressing PRC1-GFP.